

The B and Be Star Population of NGC 3766

M. Virginia McSwain^{1,2,3}

*Department of Astronomy, Yale University, P.O. Box 208101, New Haven, CT 06520-8101;
mcswain@lehigh.edu*

Wenjin Huang

*Department of Astronomy, California Institute of Technology, MC 105-24, Pasadena, CA 91125;
wenjin@astro.caltech.edu*

Douglas R. Gies, Erika D. Grundstrom⁴

Center for High Angular Resolution Astronomy, Department of Physics and Astronomy, Georgia State University, P.O. Box 4106, Atlanta, GA 30302-4106; gies@chara.gsu.edu, erika@chara.gsu.edu

Richard H. D. Townsend

Bartol Research Institute, University of Delaware, Newark, DE 19716; rhdt@bartol.udel.edu

ABSTRACT

We present multiple epochs of H α spectroscopy for 47 members of the open cluster NGC 3766 to investigate the long term variability of its Be stars. Sixteen of the stars in this sample are Be stars, including one new discovery. Of these, we observe an unprecedented 11 Be stars that undergo disk appearances and/or near disappearances in our H α spectra, making this the most variable population of Be stars known to date. NGC 3766 is therefore an excellent location to study the formation mechanism of Be star disks. From blue optical spectra of 38 cluster members and existing Strömgren photometry of the cluster, we also measure rotational velocities, effective temperatures, and polar surface gravities to investigate the physical and evolutionary factors that may contribute to the Be phenomenon. Our analysis also provides improvements to the reddening and distance of NGC 3766, and we find $E(B - V) = 0.22 \pm 0.03$ and $(V - M_V)_0 = 11.6 \pm 0.2$, respectively. The Be stars are not associated with a particular stage of main-sequence evolution, but they are a population of rapidly rotating stars with a velocity distribution generally consistent with rotation at 70 – 80% of the critical velocity, although systematic effects probably underestimate the true rotational velocities so that the rotation is much closer to critical. Our measurements of the changing disk sizes are consistent with the idea that transitory, nonradial pulsations contribute to the formation of these highly variable disks.

Subject headings: stars: emission-line, Be — open clusters and associations: individual (NGC 3766)

¹Visiting Astronomer, Cerro Tololo Inter-American Observatory. CTIO is operated by AURA, Inc. under contract to the National Science Foundation.

²NSF Astronomy and Astrophysics Postdoctoral Fellow

³Current address: Department of Physics, Lehigh University, 16 Memorial Drive East, Bethlehem, PA 18015

⁴Current address: Physics and Astronomy Department,

1. Introduction

NGC 3766 is a rich, young open cluster in the Carina spiral arm that is well known for its high content of Be stars (Slettebak 1985), and

Vanderbilt University, 1807 Station B, Nashville, TN 37235

many previous studies of this cluster have focused on the characteristics of these stars to identify their evolutionary status. The cluster has been the target of numerous photometric studies (Ahmed 1962; Yilmaz 1976; Shobbrook 1985, 1987; Moitinho et al. 1997; Piatti et al. 1998; Tadross 2001; McSwain & Gies 2005b). But despite these intensive investigations, the cluster’s age and distance remain somewhat uncertain; measurements of its age range from 14.5 to 25 Myr (WEBDA⁴; Lynga 1987; Moitinho et al. 1997; Tadross 2001), and its distance is between 1.5 and 2.2 kpc. The reddening $E(B-V)$ is between 0.16 and 0.22 (see the discussion of Moitinho et al. 1997).

Spectroscopic investigations of NGC 3766 have targeted a limited sample of cluster members, focusing primarily on the Be star and supergiant populations (Harris 1976; Mermilliod 1982 and references therein; Slettebak 1985; Levesque et al. 2005). Even the eclipsing double-lined spectroscopic binary BF Centauri (= HD 100915), a member of NGC 3766, has been largely neglected by modern spectroscopic observations (Clausen et al. 2007 and references therein). For most cluster members, no detailed information about their physical characteristics such as temperature, gravity, rotation, and metallicity are known.

In this work, we present red and blue optical spectra for both normal B-type and Be stars in the cluster. Like many prior studies of NGC 3766, our primary goal is to investigate the Be star population; but unlike other works, we achieve a more complete understanding of this subset of B stars by comparing these emission-line objects to their non-emission counterparts. Therefore we present measurements of the effective temperature, T_{eff} , surface gravity, $\log g$, and in most cases the projected rotational velocity, $V \sin i$, for 26 normal B stars and 16 Be stars in NGC 3766. We use these results to improve the known reddening and distance to the cluster. From multiple epochs of H α spectroscopy, we also investigate the variability of the circumstellar disks and estimate the disk mass loss/gain rates for 11 Be stars. Finally, we use

the observed disk masses and angular momenta to show that nonradial pulsations are a possible origin for the disks, and they probably fill during short-lived bursts of mass flow from the stellar surface.

2. Observations

We obtained spectra of NGC 3766 during multiple observing runs in 2003 March, 2005 February, 2006 May, and 2007 January–July using the CTIO Blanco 4-m telescope with the Hydra multifiber spectrograph and the CTIO 1.5-m telescope with the Cassegrain spectrograph, operated by the SMARTS Consortium. The details of all runs are summarized in Table 1. Most of the runs targeted the H α emission line profile with low spectral resolution to characterize the Be stars’ emission; however, during one run we observed the blue optical region with higher resolving power to observe numerous other H Balmer and He I line profiles and measure the physical parameters of the cluster members.

We selected the targets for each run by giving highest priority to the known Be stars in this cluster (save WEBDA No. 232, which was saturated in our photometric study). We then selected other B-type stars in the cluster by ranking them according to their y –H α color to preferentially select any weak emission stars that were not detected in our photometry (McSwain & Gies 2005a,b). All observations were performed by M. V. McSwain except the 2007 CTIO 1.5-m runs, which were taken in service mode by a SMARTS observer. For the Hydra observations, we generally began by taking short exposures and then parking the fibers used for the brightest stars to avoid saturation in the longer exposures. Not all of the known Be stars could be observed in one fiber configuration, so we took three to four exposures each of two configurations to observe all of the targets. Therefore up to eight exposures of each star were obtained with the Hydra runs. We also observed a HeNeAr comparison lamp source just before and after the set of cluster observations for wavelength calibrations. For the CTIO 1.5-m observations, we alternated each stellar observation with a Ne comparison lamp spectrum.

The CTIO 1.5-m spectra were reduced and rectified to a unit continuum using standard routines

⁴The WEBDA database is maintained by E. Paunzen and is available online at <http://www.univie.ac.at/webda/navigation.html>.

for slit spectra in IRAF. All of the Hydra spectra were zero corrected using standard routines in IRAF, and they were flat fielded, wavelength calibrated, and sky subtracted in IRAF using the *do-hydra* routine. In comparing the slit spectra and fiber spectra for many of the same objects in our data set, we find no evidence of systematic differences in the background subtraction due to cluster nebulosity. For each Hydra spectral configuration, we transformed the observations to a common heliocentric wavelength grid and co-added them to achieve good S/N for each star.

The complete sample of stars presented in this work is listed in Table 2. Column 1 gives each star’s identification number based on the assigned number in McSwain & Gies (2005b); the corresponding WEBDA numbers are given in column 2, where available. We obtained H α spectra for each of these stars during at least three epochs in most cases, and these are shown in Figures 1–3.

3. Physical Parameters from Spectral Models

3.1. $V \sin i$ Measurements

We began our investigation of each star’s physical parameters by generating a grid of synthetic, plane-parallel, local thermodynamic equilibrium (LTE) atmospheric models using the Kurucz ATLAS9 code (Kurucz 1994). We adopted solar abundances and a microturbulent velocity of 2 km s^{-1} for these stars, which corresponds to the mean microturbulence observed among late-type, main-sequence (MS) B stars (Lyubimkov, Rostopchin, & Lambert 2004). Each atmospheric model was then used to calculate a grid of model spectra using SYNSPEC (Lanz & Hubeny 2003).

For the 38 stars with available blue spectra, we made a preliminary estimate of their effective temperature and gravity, T_{eff} and $\log g$ respectively, by comparing the observed H γ , H δ , He I $\lambda 4143$, and He I $\lambda 4471$ +Mg II $\lambda 4481$ line profiles to our grid of Kurucz spectral models. To measure $V \sin i$, we compared the observed He I line profiles to the model profiles convolved with a limb-darkened, rotational broadening function and a Gaussian instrumental broadening function. We determined the best fit over a grid of values, spaced 2 km s^{-1} apart, minimizing the mean square of the devia-

tions, rms^2 . The formal error, $\Delta V \sin i$, is the offset from the best-fit value that increases the rms^2 by $2.7 \text{ rms}^2/N$, where N is the number of wavelength points within the fit region. Our measured $V \sin i$ and $\Delta V \sin i$ are listed in columns 3–4 of Table 3.

Even the He I lines may contain some weak emission in Be stars, partially filling and narrowing their line profiles. Furthermore, a number of the Be stars show evidence of narrow “shell” line components (formed in the outer disk), and the presence of a shell component may make the profile appear too narrow in some cases. Therefore we consider our $V \sin i$ measurements for the Be stars to be lower limits. However, we note that the He I lines do not exhibit obvious signs of emission among most of the Be stars, and these lines are much less susceptible to emission than the H γ or H δ lines. For the case of No. 154, a shell star with strong emission and contamination present in the He I lines, we used the Mg II $\lambda 4481$ line to measure $V \sin i$.

There are few previous measurements of $V \sin i$ for members of NGC 3766 in the literature, but we found that 10 stars in our sample were also measured by Slettebak (1985). Our $V \sin i$ measurements generally agree well, with the exception of No. 154. Slettebak found $V \sin i = 220 \text{ km s}^{-1}$ for that star, nearly double our measured value. We emphasize that the exceptionally strong He and metal lines of this shell star amplify the difficulty of measuring its $V \sin i$.

3.2. T_{eff} and $\log g$ Measurements of B stars

For the B stars with $T_{\text{eff}} < 15,000 \text{ K}$, we used the “virtual star” method of Huang & Gies (2006) to improve our T_{eff} and $\log g$ measurements. (Their virtual star is a spherically symmetric star with constant T_{eff} and $\log g$ across the stellar surface.) They generated detailed H γ line profiles using line-blanketed, LTE Kurucz ATLAS9 and SYNSPEC codes. Huang & Gies show that the H γ line strength and equivalent width can be used as starting parameters in a line profile fit to obtain unique values of T_{eff} , $\log g$, and their corresponding errors. We used their procedure to measure these quantities from our observed H γ line profiles.

Among the hotter B-type stars, non-LTE ef-

fects alter the equivalent width of the $H\gamma$ line, and thus the LTE Kurucz model line profiles systematically underestimate T_{eff} . Therefore we used the new TLUSTY BSTAR2006 grid of metal line-blanketed, non-LTE, plane-parallel, hydrostatic model spectra (Lanz & Hubeny 2007) to measure T_{eff} and $\log g$ for those stars with $T_{\text{eff}} > 15,000$ K. We used their models with solar metallicity and helium abundance and a microturbulent velocity of 2 km s^{-1} . The grid includes T_{eff} from 15,000–30,000 K in increments of 1,000 K and $\log g$ from 1.75–4.75 in increments of 0.25 dex. For these hot stars we measured T_{eff} and $\log g$ by comparing the $H\gamma$ line profile to the rotationally and instrumentally broadened model spectral line profiles at each value in the grid, minimizing rms^2 across the line region. We then refined our measurements to a higher precision using a linear interpolation between the available line profiles in the grid. Finally, we determined the errors, ΔT_{eff} and $\Delta \log g$, from the values which produce a rms^2 no more than $2.7 \text{ rms}^2/N$ greater than the minimum rms^2 . Our measurements of T_{eff} and $\log g$, with their corresponding errors, are listed in columns 5–8 of Table 3.

Many of the B stars in our sample are rapidly rotating with $V \sin i > 200 \text{ km s}^{-1}$. Such a rapidly rotating star will experience strong centrifugal forces that distort the star into an oblate spheroidal shape, as recently found for the star Regulus (McAlister et al. 2005). The surface gravity at the equator can therefore be much lower than at the poles. For such a rapid rotator, our measured T_{eff} and $\log g$ represent the average across the visible stellar hemisphere and are therefore biased toward lower values, causing the star to appear more evolved. Because the polar regions are not distorted, the surface gravity at the poles is a better indicator of the evolutionary state of the star. Huang & Gies (2006) performed detailed spectroscopic modeling of such distorted rotating stars to determine a statistical correction factor for $\log g$, averaged over all possible i , for a variety of stellar models. We made a bilinear interpolation between their models to convert our measured $\log g$ to $\log g_{\text{polar}}$ for a more accurate comparison between slow and rapid rotators.

For each B star, we also measured its mass, M_* , and radius, R_* , by interpolating between the evolutionary tracks for non-rotating stars from

Schaller et al. (1992). The errors ΔM_* and ΔR_* correspond to our measured ΔT_{eff} and $\Delta \log g$. Our results for $\log g_{\text{polar}}$, M_* , ΔM_* , R_* , and ΔR_* are also listed in Table 3, columns 9–13.

3.3. T_{eff} and $\log g$ Measurements of Be stars

Star No. 196 did not show any sign of Be emission until our most recent observations, hence we included it among the normal B stars and measured T_{eff} and $\log g$ from the $H\gamma$ line in its 2006 blue spectrum. For other Be stars in our blue spectra, the above method to measure T_{eff} and $\log g$ was not useful because the equivalent width of the $H\gamma$ line may be decreased by emission in the line, even if the line profile does not exhibit obvious signs of emission.

Our first attempt to measure the Be stars' T_{eff} and $\log g$ relied upon the He I $\lambda\lambda$ 4143, 4388, 4471 lines. We fit these three lines using TLUSTY model spectra using the same procedure described above for the $H\gamma$ line. However, these He I line strengths are less sensitive to T_{eff} , and the line wings show only a very small dependence on $\log g$. Therefore these line fits resulted in very large errors for both parameters in many cases. Furthermore, the Be disks contribute continuum flux that dilutes the apparent strength of the He I lines, so $\log g$ values measured from these lines do not always agree well.

To improve our T_{eff} measurements for the Be stars, we turned to available Strömgren m_1 , c_1 , and β indices for our targets (Shobbrook 1985, 1987; WEBDA). Several temperature relations for Strömgren indices are available in the literature (see Napiwotzki et al. 1993 and references therein), so we began by using our normal B-type stars with $T_{\text{eff}} > 15000$ K as calibrators to determine the best relation for our data. We adopted the reddening value of $E(b - y) = 0.15$ (corresponding to $E(B - V) = 0.2$) for NGC 3766 (Shobbrook 1985; Moitinho et al. 1997). Eight stars in our sample (Nos. 16, 42, 49, 54, 57, 161, 170, and 196) have available Strömgren indices as well as T_{eff} measured from our $H\gamma$ line fits, and Napiwotzki et al. provide eight calibrators with well-known $T_{\text{eff}} > 15000$ K (measured from their absolute integrated stellar flux) and available Strömgren data. For these 16 B stars, we found the best overall agreement using the temperature

relation from Balona (1984), shown in Figure 4. However, we found that T_{Balona} systematically underestimated T_{eff} , and a correction factor was necessary to improve their agreement. We performed a linear fit to the data and found the relationship

$$T_{\text{eff,fit}} = 1.052 T_{\text{Balona}} - 359.636 \text{ K} \quad (1)$$

(excluding one outlying point from Napiwotzki et al. 1993). The slope of this correction is virtually identical to the values found by both Gies & Lambert (1992) and Cunha & Lambert (1994). After applying this correction, we found a mean scatter of 264 K from our two independent measurements of T_{eff} for the B stars in NGC 3766.

T_{Balona} relies upon the dereddened c_0 index as well as the narrow-band β magnitude, so determining an accurate temperature for the Be stars also requires confidence in β . However, the Be stars' emission makes the β magnitude highly unreliable. Therefore we used the B star calibrators from our sample (listed above) to investigate several (c_0, β) relations in the literature (Crawford 1978; Balona & Shobbrook 1984). The (c_0, β) diagram is essentially a H-R diagram that reveals temperature and evolutionary trends in a population. In Figure 5, we show that the values of c_0 and β for these B-type calibrators generally agree with the relations for luminosity class III and V stars from Balona & Shobbrook (1984). However, the calibration stars have $3.43 < \log g < 3.98$ ($3.49 < \log g_{\text{polar}} < 4.17$) since these hot stars are evolving along the MS, and neither (c_0, β) relation can be applied to the entire population. Therefore we performed a linear fit to account for the range in evolution, and we found the relationship

$$\beta_{\text{fit}} = 0.417 c_0 + 2.545 \quad (2)$$

among the B stars in NGC 3766 with $T_{\text{eff}} > 15000$ K. The mean scatter between β_{fit} and the measured β is 0.010, which implies an additional error of 144 K in T_{eff} using the corrected T_{Balona} relation above.

Shobbrook (1985, 1987) presented Strömgren photometry for nine Be stars that have accompanying blue spectra in this work (excluding No. 196, which we used as a calibrator) and four Be stars with only red spectra in this work. Thus we measured T_{eff} for all 13 of these Be stars using the adopted β_{fit} and the corrected T_{Balona}

as described above. We adopt a total error of $(264^2 + 144^2)^{0.5} = 301$ K for T_{eff} measured with this method, and the results are listed in columns 5–6 of Table 3.

Using this technique, only the “shell” Be star No. 154 results in $T_{\text{eff}} < 15000$ K. The comparisons between T_{Balona} and our independently measured T_{eff} are less reliable below this temperature threshold, hence we used only B star calibrators with $T_{\text{eff}} > 15000$ K. However, spectroscopy is even less likely to produce accurate measurements for No. 154 since its spectrum is contaminated by He I emission and the metal lines are exceptionally strong due to the disk’s edge-on orientation. Therefore we include in Table 3 its T_{eff} from the corrected relations of Balona (1984), but the errors are somewhat higher than for the other Be stars.

The values of $\log g$ are more strongly dependent on β , so we were reluctant to use our β_{fit} with the Strömgren relation for $\log g$ given by Balona (1984). Instead, we used the calculated T_{eff} to determine the Be stars’ bolometric corrections, BC, from Lanz & Hubeny (2007), at first assuming $\log g = 4.0$. For the cooler star No. 154, we interpolated the BC from the values for MS stars given by Cox (2000). We calculated each stellar radius, R_* , and luminosity, L_* , using the measured T_{eff} , BC, V magnitude (Shobbrook 1985, 1987; WEBDA), distance modulus $(V - M_V)_0 = 11.73 \pm 0.33$ (Moitinho et al. 1997), and $E(B - V) = 0.2 \pm 0.1$ (Shobbrook 1985; Moitinho et al. 1997). We measured the stellar mass, M_* , from the computed T_{eff} and L_* by interpolating between the evolutionary tracks of Schaller et al. (1992). Finally, we obtained a preliminary value of $\log g$ from M_* and R_* . Since the BC is weakly dependent on $\log g$, we improved the BC from the initial estimate and iterated to compute the final $\log g$. We adopt a formal error in $\log g$ computed from ΔT_{eff} and the quoted errors in $(V - M_V)_0$ and $E(B - V)$.

We note that the scatter between the calibrators’ $\log g_{\text{polar}}$ and their Strömgren $\log g$ is identical to the formal error. Based on this good agreement, we do not perform any further correction to obtain $\log g_{\text{polar}}$ for the Be stars measured with this technique. However, we show below that the Be stars are more rapidly rotating than the normal B stars, which may make them appear slightly

more evolved and artificially brightened. Thus these values of $\log g_{\text{polar}}$ are lower limits. The final parameters for these Be stars are listed in Table 3.

Two Be stars in our sample of blue spectra have no available Strömgren data in the literature. By coincidence, these stars (Nos. 31 and 127) have two of the best T_{eff} and $\log g$ measurements from our preliminary He I line fits. Therefore we adopt the mean measurements from the He I $\lambda\lambda$ 4143, 4388, 4471 lines, with a formal error determined from the values which produce a rms^2 no more than $2.7 \text{rms}^2/N$ greater than the minimum rms^2 . A contour plot of the errors in T_{eff} and $\log g$ for No. 31 is shown in Figure 6, and the final values are listed in Table 3. We determined their $\log g_{\text{polar}}$ using the same method as the B stars.

3.4. Discussion of Physical Parameters

The resulting values of T_{eff} and $\log g_{\text{polar}}$ are plotted in Figure 7 with the corresponding evolutionary tracks for non-rotating stars from Schaller et al. (1992). The symbol sizes are proportional to $V \sin i$ to investigate the relation between rotation and the apparent evolutionary state of each star, but no trends are observed. Also in Figure 7, we plot the isochrones for 25–50 Myr populations from Lejeune & Schaerer (2001). Our distribution of T_{eff} and $\log g_{\text{polar}}$ are generally consistent with a population within this range, indicating an age slightly greater than previous estimates for NGC 3766.

The masses of the rapidly rotating stars may be overestimated since the evolutionary tracks do not account for rotation. We minimize this effect by using the corrected $\log g_{\text{polar}}$ for all stars, but slight mass differences may still be present since rapid rotation is expected to alter the evolution (Heger & Langer 2000; Meynet & Maeder 2000). McAlister et al. (2005) found a small, 15% mass discrepancy for the rapid rotator Regulus when comparing its mass derived from non-rotating evolutionary tracks and its true mass from a detailed spectroscopic and interferometric analysis.

We find that the Be stars are generally among the hotter stars in our sample, consistent with our earlier findings from a photometric investigation of 48 open clusters that Be stars are preferentially found among the more luminous cluster members

(McSwain & Gies 2005b). There are no systematic differences between the $\log g_{\text{polar}}$ of the Be star and normal B star populations of the cluster, indicating that the Be stars in NGC 3766 are distributed across a range of $\log g_{\text{polar}}$ and are not associated with any particular stage of the MS evolution of B-type stars. This is also consistent with our earlier results (McSwain & Gies 2005b) and with Zorec et al. (2005), who performed an evolutionary study of field Be stars. On the other hand, Levenhagen & Leister (2006) found that field Be stars are preferentially found at later stages of the MS evolution. They did not perform any corrections for gravity darkening among these rapid rotators, so their Be stars may be found closer to the zero-age MS than their results suggest.

4. Rotational Velocities

Be stars are often described as a population of rapidly rotating B-type stars with a true rotational velocity V_{rot} comparable to the critical velocity V_{crit} . (Note that V_{rot} should not be confused with V in our measured $V \sin i$, which may be subject to systematic errors such as gravitational darkening or weak emission in the He I lines.) However, a recent study by Cranmer (2005) has cast some doubt on their fast rotation. He compared available $V \sin i$ measurements in the Yudin (2001) database of Oe, Be, and Ae stars to the predicted distribution of $V \sin i$ accounting for gravity darkening, limb darkening, and observational effects. He found that the Be stars of the Yudin database have intrinsic rotations between 40–100% critical, with more early-type Be stars having significantly subcritical rotation. However, the Yudin database is a compilation of measurements from many different authors and instrumental setups, and therefore the available $V \sin i$ may contain significant systematic differences. Our measurements of $V \sin i$ rely upon data of identical origin and measurements of the same spectral lines in nearly every case. Therefore we have greatly reduced the systematic differences among our Be star measurements, and our measurements are also a reliable comparison of Be stars relative to normal B stars.

A rotationally distorted star has an equatorial radius $R_e = 1.5R_p$ in the Roche approximation; here, R_p is the star’s polar radius. For simplicity, we assume R_p is equal to the radius R_* derived

from the position in Figure 7 and given in Table 3. The resulting critical velocity is

$$V_{\text{crit}} = \sqrt{\frac{GM_{\star}}{R_{\text{e}}}} \quad (3)$$

and is included in Table 3. A small mass discrepancy, as found for Regulus (McAlister et al. 2005), will not affect V_{crit} significantly since a 15% error in mass produces only a 4% error in V_{crit} . Here we investigate the rotational properties of several edge-on Be stars in our sample and compare the distribution of Be star velocities with the normal B stars to compare the two populations.

Two Be stars in our sample, Nos. 92 and 139, show $\text{H}\alpha$ emission only in the line wings, with a deep absorption profile, suggesting the disks are observed nearly edge-on. This is probably a good assumption for No. 139 since it has $V/V_{\text{crit}} \geq 0.7$. However, No. 92 may not be edge on since its $\text{H}\alpha$ profiles between 1985–1990 (Balona et al. 1991) do not resemble the profiles we observe. Either the disk is precessing or other structural changes have occurred. A third star, No. 154, exhibits a shell spectrum with strong metal lines that also suggests an edge-on orientation.

If we assume that all of the Be stars have $V/V_{\text{crit}} = 0.95$, then our measured $V \sin i$ indicate that stars 92, 139, and 154 have $i = 34^\circ$, 48° , and 15° , respectively. Assuming a slower, $V/V_{\text{crit}} = 0.70$ increases the derived values to $i = 49^\circ$, 90° , and 20° respectively, but the low i for Nos. 92 and 154 are still inconsistent with the observed line profiles. However, if we fix $i = 80^\circ$ for all three stars, we find that $V/V_{\text{crit}} = 0.53$ for No. 92, $V/V_{\text{crit}} = 0.71$ for No. 139, and $V/V_{\text{crit}} = 0.24$ for No. 154. Townsend et al. (2004) show that measured $V \sin i$ may be too low due to gravitational darkening in highly distorted, rapidly rotating stars. But even accounting for a 20–33% underestimate in $V \sin i$ for Nos. 92 and 154, we do not find that these two Be stars are near critical rotation.

The distributions of $V \sin i$ for both the Be stars and normal B stars are plotted in Figure 8. Although this sample of 38 stars is small, this study is the first to measure $V \sin i$ for both groups using a consistent method and a uniform data set. Our measured $V \sin i$ for the Be stars may be only lower limits, but we clearly find that the Be stars of NGC 3766 are more rapidly rotating than the

normal B star population. In Figure 8, we also include theoretical distributions of two uniform, rapidly rotating populations with $V = 0.7 V_{\text{crit}}$ and $V = 0.8 V_{\text{crit}}$, assuming $V_{\text{crit}} = 386 \text{ km s}^{-1}$ (the mean value among the Be stars, excluding No. 154 due to its large measurement errors). The distribution of Be stars is consistent with $0.7 V_{\text{crit}} < V < 0.8 V_{\text{crit}}$ in most cases. However, if each measured $V \sin i$ is underestimated by 20–33% due to gravitational darkening, as claimed by Townsend et al. (2004), the distribution of Be star velocities is consistent with $V_{\text{rot}} \geq 0.84 V_{\text{crit}}$. Nos. 92 and 154 represent significant exceptions to this rule, as discussed above.

5. Other Results from Spectra

We do not wish to broaden the scope of this paper to discuss the radial velocities and helium abundances observed in our spectra. However, we found several instances that suggest these topics are worth exploring in future studies of NGC 3766.

Figure 1 includes the variable $\text{H}\alpha$ profile of No. 61. The absorption line is deep and narrow in 2005, yet wide and shallow in 2006 and 2007. These line profile changes are not consistent with a Be star, and they probably indicate line blending in a double-lined spectroscopic binary (SB2). Likewise, No. 197 may be an SB2. We observed double Mg II 4481 lines in 2006, and Figure 3 shows a large wavelength shift in its $\text{H}\alpha$ line profile between 2005–2006. There is possible line blending visible in the 2005 and 2007 $\text{H}\alpha$ profiles.

We measured the physical parameters of the B stars using spectral models that have solar helium abundances, and most were consistent with a solar abundance. However, we noticed a large number that have abnormal He abundances; Nos. 41, 55, 94, 118, and 178 appear to be He strong, while Nos. 126, 129, 170, 173, and 197 appear He weak. Since all cluster members are expected to have the same He abundance, this may indicate widespread magnetic fields in the cluster which can produce nonuniform distributions of He across the stellar photospheres (see discussion of Huang & Gies 2006). The He weak stars may also be binaries with cooler companions adding flux but diluting the appearance of the He I lines.

Finally, we used our spectra to reinvestigate the reddening and distance to NGC 3766. For

the nonemission B stars with $\log g_{\text{polar}} > 3.9$, we used the MS relation of Harmanec (1988) to assign a spectral type to each star based on its measured T_{eff} . We then used the MS relation of Wegner (1994) to find the stars' intrinsic colors, $(B - V)_0$. Observed $B - V$ colors were obtained from WEBDA. For the 17 B-type, MS stars in our sample, we found $E(B - V) = 0.223 \pm 0.030$. We then used the B stars' V magnitude (WEBDA), BC (Lanz & Hubeny 2007, Malagnini et al. 1986), and our measured R_* to compute the distance modulus, $(V - M_V)_0$. The resulting $(V - M_V)_0 = 11.42 \pm 0.15$. To determine the mean $(V - M_V)_0$, we excluded No. 45 with a somewhat lower $(V - M_V)_0$ of 10.3, probably a foreground star.

While the B stars of NGC 3766 are rotating more slowly than the Be stars, they have a mean $V \sin i / V_{\text{crit}} = 0.5$. Assuming a random distribution of i , this corresponds to a mean $V / V_{\text{crit}} = 0.7$. Such rapidly rotating stars are probably rotationally distorted with surface areas ≈ 1.2 times larger than spherical star with $R_* = R_{\text{polar}}$, causing them to appear overluminous. The distance modulus is then underestimated by a factor of $2.5 \log 1.2 = 0.21$. With a realistic distribution of V and i , this correction may not be appropriate for all stars, and the range in $\Delta(V - M_V)_0$ is $0.02 - 0.30$ for $0.28 \leq V / V_{\text{crit}} \leq 0.83$. We apply this correction to find a final $(V - M_V)_0 = 11.6 \pm 0.2$ for NGC 3766, corresponding to a distance of $1.9 - 2.3$ kpc. Our new values of $E(B - V)$ and $(V - M_V)_0$ are highly consistent with previous results for this cluster.

6. Be Star Variability

While the long term $H\alpha$ variability of Be stars has often been noted in the literature (e.g. Porter & Rivinius 2003), few studies have attempted long term monitoring of a large sample of Be stars to quantify their variability. Hubert & Floquet (1998) investigated 273 bright Be stars with $V < 7.5$ that were observed by Hipparcos between 1989 August and 1993 August. They found that early type Be stars exhibit a very high degree of variability while most late Be stars maintained a constant magnitude during the duration of the Hipparcos mission. They also identified 14 Be stars with recurrent short-lived outbursts ($0.06 \leq \Delta H_p \leq 0.3$ over timescales

of 50–500 days) and 8 with long-lived outbursts ($\Delta H_p \geq 0.12$ over timescales of > 500 days) in the sample. However, the Hipparcos magnitude, H_p , covers a broad waveband ranging from 3400 to 8500 Å, and it traces large scale variations in the continuum from scattered light associated with the disk. $H\alpha$ spectroscopy is better suited to measuring variations over a larger dynamic range in the disks of Be stars of all spectral types.

Figures 1–3 show the $H\alpha$ line profile variations of all 47 stars in our spectroscopic sample. We were intrigued to discover a new Be star (No. 130) in NGC 3766 based on our comparison of its $H\alpha$ line profiles. In 2005 February, the absorption line was broad and shallow, with some bumps that suggest a weak emission disk, nonradial pulsations, or simply noise. By 2006 May, however, the depth of the line had increased while its width remained nearly the same, but a slight asymmetry in the line suggested that perhaps a very weak disk may still have been present. The line remained in absorption during our most recent 2007 observations. While an inverse relation between the line width and depth is associated with line blending in an SB2, the observed variations in No. 130 cannot be attributed to such line blending. Instead, the three sets of observations indicate the presence of a weak circumstellar disk in 2005 that largely disappeared by 2006.

In fact, we were startled to find that a total of 11 Be stars in our sample exhibit significant changes in their disk state between 2003–2007. Stars 25, 31, 73, 83, 92, 98, 119, 130, 133, 139, and 196 each show $H\alpha$ in absorption in at least one of the four epochs available, yet each star also experiences at least one epoch when the $H\alpha$ line is partially or fully filled with emission. These observations suggest that the mechanism responsible for the disk formation is unstable over timescales of only a few years, consistent with the results of Hubert & Floquet (1998). The disk growth of No. 31 during 2007 reveals that the disk formation can be very rapid, only requiring a few days or weeks, as observed in other Be stars (e.g. Grundstrom et al. 2007). However, the high fraction of Be stars that show significant variability in a single cluster is unprecedented, and the cluster should be monitored with increased frequency to measure an accurate timescale of the disk state changes.

Five additional Be stars (47, 127, 154, 198, and 200) show H α emission in every observation, although the emission strength is usually variable. Such variations in H α emission strength are typical among Be stars.

To quantify the observed changes in the Be star disks, we measured the equivalent width, W_λ , of the H α line in each of our red spectra by normalizing each spectrum to a unit continuum and integrating over the line profile. Columns 3–6 of Table 2 give the measured values of W_λ for each spectrum. The error in each measurement is about 10% due to noise in the continuum region.

With multiple epochs of H α observations available for so many variable Be stars, it is worthwhile to estimate the changing size of the circumstellar disks. Grundstrom & Gies (2006) describe a simple model to measure the ratio of the projected effective disk radius to the stellar radius, R_{disk}/R_\star , and the density at the base of the disk, ρ_0 , using W_λ and T_{eff} as input parameters. We determined the disk inclination i by assuming that each star is rotating with V at 70% of V_{crit} in most cases. We also assumed a disk truncation radius of 100 R_\star , the nominal value unless a close binary companion is present. The disk temperature is assumed to be constant at 0.6 T_{eff} .

To estimate the total masses of the disks, we used an axisymmetric, isothermal density distribution,

$$\rho(r, z) = \rho_0 \left(\frac{R_\star}{r} \right)^n \exp \left[-\frac{1}{2} \left(\frac{z}{H(r)} \right)^2 \right] \quad (4)$$

(Carciofi & Bjorkman 2006) and a radial density exponent $n = 3$, typical of other Be star disks (Gies et al. 2007). The scale height of the disk is

$$H(r) = H_0 \left(\frac{r}{R_\star} \right)^\beta, \quad (5)$$

where

$$H_0 = \frac{a}{V_{\text{crit}}} R_\star, \quad (6)$$

$$a = \sqrt{\frac{kT}{\mu m_{\text{H}}}}, \quad (7)$$

and $\beta = 1.5$ for an isothermal disk (Bjorkman & Carciofi 2005; Carciofi & Bjorkman 2006).

The resulting disk properties are listed in Table 4 for each Be star with an available T_{eff} measurement. The time of each observation is listed in column 2, and the dates for the CTIO 4m+Hydra observations are less precise since these $W_{\text{H}\alpha}$ were measured from co-added spectra rather than individual spectra obtained with the CTIO 1.5m telescope. Our determined values for i , ρ_0 , R_{disk}/R_\star , and M_{disk} are listed in columns 4–7.

Certainly, these disk measurements should be viewed with caution since the true density profiles may be quite different from the assumed distribution. The disk density exponent may be different from our assumed value of $n = 3$, and the resulting mass estimates may differ from our results by orders of magnitude. Contemporaneous optical and infrared spectra have also revealed evidence of density waves that alter the azimuthal disk structure (Wisniewski et al. 2007). Finally, the disks are likely not isothermal as we assumed, and the true thermal structure may be very complex (Carciofi & Bjorkman 2006). Therefore the processes associated with the H α emission profile are much more complex than assumed in the model of Grundstrom & Gies (2006), but by using their simple model we obtain relative estimates of the variations in disk base density that are sensible provided the disk density exponent is assumed constant in time.

7. Disk Formation by Nonradial Pulsations

The estimates for ρ_0 and M_{disk} above are not sensitive to i and offer a consistent method to measure changes in the size of the disks. Thus we can estimate the disk growth rate (or dissipation rate), $\Delta M_{\text{disk}}/\Delta t$. Our generally sparse observations cannot determine whether $\Delta M_{\text{disk}}/\Delta t$ is constant or highly variable over timescales less than one year; however there is an indication from the two closely spaced observations of Nos. 25 and 31 that the disk size can change rapidly. We provide our measured $\Delta M_{\text{disk}}/\Delta t$ between each pair of observations in Table 4. The long-term buildup rates are comparable for every Be star in our sample, hinting that all of the disks might be formed by the same mechanism. Finally, the buildup and dissipation rates are also comparable in magnitude.

Many Be stars are known to exhibit nonradial pulsations (NRP) with the mode $\ell = 2$, $m = \pm 2$ (Rivinius et al. 2003), and such pulsations are commonly proposed as the source of kinetic energy to inject material into the disk (Porter & Rivinius 2003). The $m = +2$ pulsational mode is retrograde, and naively it will counteract the rotational velocity of the star and hinder disk formation. However, Townsend (2005) shows that retrograde mixed modes behave in a way that could contribute to Be disk formation. Although their phase velocity is retrograde, their group velocity is prograde. The density enhancements occur when the pulsational velocity perturbation is in the same direction as the rotation – a configuration favorable to mass ejection. He also found the mixed mode instability strip likely overlaps with the temperatures and spectral types of known Be stars if their rotation is nearly critical.

Observations of known β Cephei pulsators and slowly pulsating B stars indicate that their pulsation modes have velocity amplitudes on the order of 10 km s^{-1} (combining the radial, azimuthal, and longitudinal components of the total velocity vector; De Ridder 2001). Owocki (2005) shows that the velocity needed for ejection into the disk is $\Delta V_{\text{orb}} = V_{\text{crit}} - V_{\text{rot}}$. For a weak atmospheric process such as NRP, the atmospheric sound speed $a \sim 12 \text{ km s}^{-1}$ must be comparable to ΔV_{orb} . If we assume that the stars have $V_{\text{rot}} = 0.95 V_{\text{crit}}$, then $\Delta V_{\text{orb}} \sim 20 \text{ km s}^{-1}$, highly comparable to a and the observed pulsation velocities in other NRP stars (De Ridder 2001). As we show above, this assumption of near critical rotation is reasonable for most of the Be stars in NGC 3766.

To compare the NRP velocity with the outflow velocity required to fill the Be disks, we use the equation of mass continuity for an equatorial outflow with velocity $v_{\text{r,eq}}$:

$$\sigma(r) = \frac{\Delta M_{\text{disk}} / \Delta t}{2\pi r v_{\text{r,eq}}} \quad (8)$$

where the surface density of the disk is

$$\sigma(r) = \int_{-\infty}^{\infty} \rho(r, z) dz. \quad (9)$$

Since we remove the vertical dependence of the disk density by using its surface density, this method effectively assumes that all of the material leaves the star through a cylindrical surface

of arbitrary height. For a disk reaching down to the stellar surface, the mass must flow across this surface, so we use the surface density at the stellar surface, $\sigma(R_{\text{eq}})$, in the continuity relation. Since the $\ell = 2$, $m = \pm 2$ modes have the greatest pulsational amplitude at the stellar equator, where the effective surface gravity is also a minimum, it is reasonable to expect the majority of the disk material to be ejected from the equator in the NRP model. The observed disk formation rates are generally $\Delta M_{\text{disk}} / \Delta t = 10^{-12} - 10^{-11} M_{\odot} \text{ yr}^{-1}$ with $\rho_0 = 10^{-12} \text{ g cm}^{-3}$ from Table 4. This implies a very slow surface flow on average, $v_{\text{r,eq}} \sim .01 - 0.1 \text{ km s}^{-1}$. However, a few observations reveal that the surface flow can be an order of magnitude faster, but this is still consistent with NRP.

Likewise, we use our observed disk densities to demonstrate that NRP are a capable source of angular momentum, L , for disks. The rotational inertia, I , of a thin disk shell is given by

$$I(r) = 2\pi r^3 \sigma(r) dr \quad (10)$$

and the total angular momentum of the disk, extending from the stellar surface to $100R_{\star}$, is

$$L = \int_{R_{\text{eq}}}^{100R_{\star}} I(r) \omega(r) dr. \quad (11)$$

where $\omega(r) = (GM_{\star})^{0.5} r^{-1.5}$ is the angular velocity of a Keplerian disk. We find that $L \sim 10^{43} - 10^{44} \text{ g cm}^2 \text{ s}^{-1}$ for the observed disks, with $\Delta L / \Delta t \sim 10^{32} - 10^{36} \text{ g cm}^2 \text{ s}^{-2}$. Osaki (1986) shows that the angular momentum flux in the equatorial plane due to NRP with $\ell = 2$, $m = \pm 2$ is given by

$$\frac{dL}{dt} = 2\pi R_{\text{eq}}^2 \sigma(R_{\text{eq}}) A^2 k \sin \delta. \quad (12)$$

Here, A and $2Ak$ are the radial and azimuthal amplitudes of pulsation, respectively, and δ is the phase shift between the two velocity components. Thus we find that a small azimuthal pulsation with $2Ak \sim 0.01 - 0.1 \text{ km s}^{-1}$ can, in principle, provide enough angular momentum to eject material into the observed disks, and both the radial and azimuthal amplitudes are highly consistent with the observed pulsation amplitudes of other B stars with NRP (De Ridder 2001).

Our results suggest that the NRP may be a transitory phenomenon for the Be stars, and

the disks may fill substantially during short periods of surface activity. Evidence for changing pulsational modes among several stars in NGC 3766 has been observed by Balona et al. (1991), van Vuuren et al. (1988), and Balona & Engelbrecht (1986). They found periodic light curve variations in several Be stars in NGC 3766 (our Nos. 47, 92, 133, 154, and 200). Additional Be stars, our Nos. 98, 130, 198 also exhibit light curve variations that are possibly periodic. In several cases, the shapes and possibly periods of the light curves change with timescales of only a few weeks. Balona et al. (1991) argue that this is due to magnetic fields, but the light curves are not qualitatively similar to variations observed in other magnetic stars, such as the prototype σ Ori E (Oksala & Townsend 2007). The changing light curves among NGC 3766 members are probably more consistent with changes in active pulsation modes over short timescales.

8. Conclusions

Our spectroscopic analysis of NGC 3766 has revealed that Be stars may be much more common than we originally thought. In our photometric study of NGC 3766 (McSwain & Gies 2005b), we found up to 13 Be stars (5 definite, 8 uncertain) out of an expected 191 B-type stars, not counting the one Be star that saturated our photometry. The new total of 16 Be stars is 23% greater. Among these 16 Be stars, 2–5 of them appear to have almost no disk at any given time, and an additional 2–4 have extremely subtle emission in their H α line profile that could easily be mistaken for other phenomena (such as NRP manifesting themselves as bumps moving across the line or SB2 line blending). Therefore 25–50% of the Be stars may go undetected in a single spectroscopic observation, and photometric snapshots are even less likely to discern such weak emitters. We note four stars (Nos. 27, 45, 49, and 77) that were found to be possible or likely Be stars in the photometric study by Shobbrook (1985, 1987), but they never showed emission during our observations and thus remain unconfirmed. The existence of transitory, weak disks (especially Nos. 130 and 196) could mean that many more Be stars are waiting to be discovered.

For our total sample of 48 Southern open clus-

ters in our photometric survey, we found a low Be fraction of 2–7% (McSwain & Gies 2005b). Considering the very weak disks that are observed in NGC 3766 and the exceptionally high variability among the cluster’s Be population, the total fraction of Be stars could be much greater. We are currently performing a similar spectroscopic study of several other clusters from our survey, and we will address those results in a future paper.

While the Be stars of NGC 3766 are not distinguishable from normal B-type stars by their evolutionary states, they do form a population of rapidly rotating stars. With two exceptions, their measured velocities are consistent with a uniform population of rapid rotators having $V = 0.7 - 0.8 V_{\text{crit}}$. Gravitational darkening and weak emission in the He I lines may mean that these velocities are underestimated by as much as 33% (Townsend et al. 2004), so the true V_{rot} is probably at least $0.84 V_{\text{crit}}$. From the measured changes in the disks’ masses and angular momenta, NRP are a capable source for the mass flow into the equatorial plane. The pulsations may be a transitory phenomenon, however, and the variable nature of the Be stars probably reflects dramatic changes in the surface activity.

We thank the referee, Phil Massey, for providing comments that improved this work. Also, we are grateful to Giovanni Carraro, Mark Pinsonneault, and Svetlana Hubrig for helpful discussions that contributed to this work. We are grateful to Yale University and the SMARTS Consortium for providing observing time at the CTIO 1.5m telescope. This research has made use of the WEBDA database, operated at the Institute for Astronomy of the University of Vienna. MVM was supported by an NSF Astronomy and Astrophysics Postdoctoral Fellowship under award AST-0401460. This work was also supported by the National Science Foundation under grant AST-0606861 (DRG) and by NASA under grant LTSA/NNG05GC36G (RHDT).

Facilities: CTIO.

REFERENCES

- Ahmed, F. 1962, Pub. Royal Obs. Edinburgh, 3, 60
- Balona, L. A. 1984, MNRAS, 211, 973

- Balona, L. A., & Engelbrecht, C. A. 1986, *MNRAS*, 219, 131
- Balona, L. A., & Shobbrook, R. R. 1984, *MNRAS*, 211, 375
- Balona, L. A., Sterken, C., & Manfroid, J. 1991, *MNRAS*, 252, 93
- Bjorkman, J. E., & Carciofi, A. C. 2005, in *The Nature and Evolution of Disks Around Hot Stars* (A.S.P. Conf. Ser.), ed. R. Ignace and K. Gayley (San Francisco: ASP), 337, 75
- Carciofi, A. C., & Bjorkman, J. E. 2006, *ApJ*, 639, 1081
- Clausen, J. V., Helt, B. E., Giménez, A., Vaz, L. P. R., García, J. M., Olsen, E. H., & Southworth, J. 2007, *A&A*, 461, 1065
- Cox, A. N. 2000, *Allen's Astrophysical Quantities* (4th ed.; New York: Springer-Verlag)
- Cranmer, S. R. 2005, *ApJ*, 634, 585
- Crawford, D. L. 1978, *AJ*, 83, 48
- Cunha, K., & Lambert, D. L. 1994, *ApJ*, 426, 170
- De Ridder, J. 2001, Ph.D. thesis, Katholieke Universiteit Leuven
- Gies, D. R., et al. 2007, *ApJ*, 654, 527
- Gies, D. R., & Lambert, D. L. 1992, *ApJ*, 387, 673
- Grundstrom, E. D., & Gies, D. R. 2006, *ApJ*, 651, L53
- Grundstrom, E. D., et al. 2007, *ApJ*, 660, 1398
- Harmanec, P. 1988, *Bull. Astron. Inst. Cz.*, 39, 329
- Harris, G. L. H. 1976, *ApJS*, 30, 451
- Heger, A., & Langer, N. 2000, *ApJ*, 544, 1016
- Huang, W., & Gies, D. R. 2006, *ApJ*, 648, 591
- Hubert, A. M., & Floquet, M. 1998, *A&A*, 335, 565
- Kurucz, R. L. 1994, *Kurucz CD-ROM 19, Solar Abundance Model Atmospheres for 0, 1, 2, 4, 8 km/s* (Cambridge: SAO)
- Lanz, T., & Hubeny, I. 2003, *ApJS*, 146, 417
- Lanz, T., & Hubeny, I. 2007, *ApJS*, 169, 83
- Lejeune, T., & Schaerer, D. 2001, *A&A*, 366, 538
- Levenhagen, R. S., & Leister, N. V. 2006, *MNRAS*, 371, 252
- Levesque, E. M., Massey, P., Olsen, K. A. G., Plez, B., Josselin, E., Maeder, A., & Meynet, G. 2005, *ApJ*, 628, 973
- Lynga, G. 1987, *Catalogue of Open Cluster Data* (5th Ed.), Lund Obs. Pub., online at VizieR no. VII/92A
- Lyubimkov, L. S., Rostopchin, S. I., & Lambert, D. L. 2004, *MNRAS*, 351, 745
- Malagnini, M. L., Morossi, C., Rossi, L., & Kurucz, R. L. 1986, *A&A*, 162, 140
- McAlister, H. A., et al. 2005, *ApJ*, 628, 439
- McSwain, M. V., & Gies, D. R. 2005a, *ApJ*, 622, 1052
- McSwain, M. V., & Gies, D. R. 2005b, *ApJS*, 161, 118
- Mermilliod, J.-C. 1982, *A&A*, 109, 48
- Meynet, G., & Maeder, A. 2000, *A&A*, 361, 101
- Moitinho, A., Alfaro, E. J., Yun, J. L., & Phelps, R. L. 1997, *AJ*, 113, 1359
- Napiwotzki, R., Schoenberner, D., & Wenske, V. 1993, *A&A*, 268, 653
- Oksala, M., & Townsend, R. 2007, in *Active OB Stars: Laboratories for Stellar & Circumstellar Physics* (A.S.P. Conf. Ser.), ed. S. Stefl, S. Owocki, and A. Okazaki (San Francisco: ASP), 361, 476
- Osaki, Y. 1986, *PASP*, 98, 30
- Owocki, S. 2005, in *The Nature and Evolution of Disks Around Hot Stars* (A.S.P. Conf. Ser.), ed. R. Ignace and K. Gayley (San Francisco: ASP), 337, 101
- Piatti, A. E., Claria, J. J., & Bica, E. 1998, *ApJS*, 116, 263
- Porter, J. M., & Rivinius, T. 2003, *PASP*, 115, 1153

- Rivinius, T., Baade, D., & Štefl, S. 2003, *A&A*, 411, 229
- Schaller, G., Schaerer, D., Meynet, G., & Maeder, A. 1992, *A&AS*, 96, 269
- Schild, R. E. 1970, *ApJ*, 161, 855
- Shobbrook, R. R. 1985, *MNRAS*, 212, 591
- Shobbrook, R. R. 1987, *MNRAS*, 225, 999
- Slettebak, A. 1985, *ApJS*, 59, 769
- Tadross, A. L. 2001, *New Astronomy*, 6, 293
- Townsend, R. H. D. 2005, *MNRAS*, 364, 573
- Townsend, R. H. D., Owocki, S. P., & Howarth, I. D. 2004, *MNRAS*, 350, 189
- Tycner, C., et al. 2006, *AJ*, 131, 2710
- van Vuuren, G. W., Balona, L. A., & Marang, F. 1988, *MNRAS*, 234, 373
- Wegner, W. 1994, *MNRAS*, 270, 229
- Wisniewski, J. P., Kowalski, A. F., Bjorkman, K. S., Bjorkman, J. E., & Carciofi, A. C. 2007, *ApJ*, 656, L21
- Yilmaz, F. 1976, *A&AS*, 26, 1
- Yudin, R. V. 2001, *A&A*, 368, 912
- Zorec, J., Frémat, Y., & Cidale, L. 2005, *A&A*, 441, 235

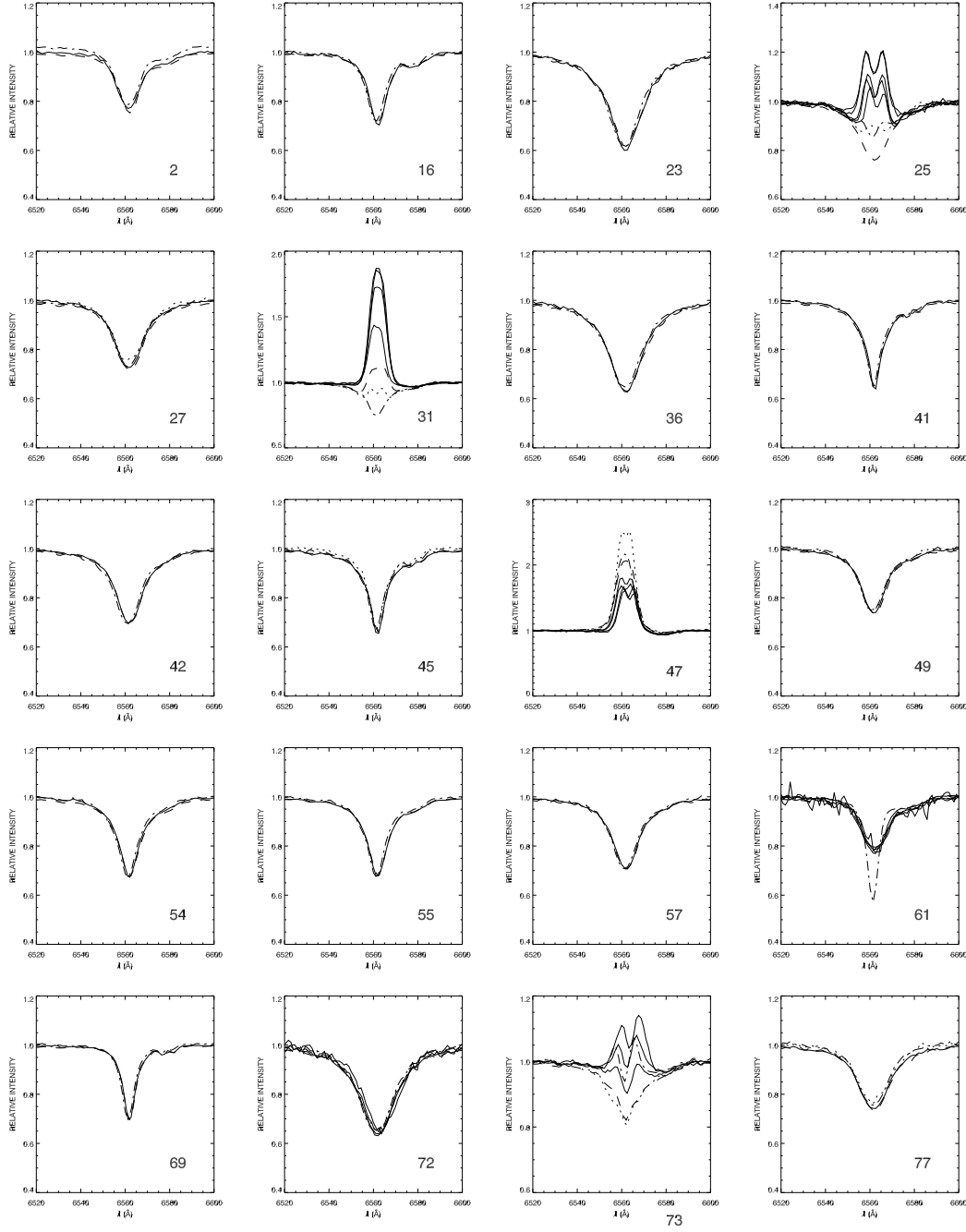


Fig. 1.— $H\alpha$ profiles, labeled by MG ID number. Spectra from 2003, where available, are shown with *dotted lines*, spectra from 2005 are shown with *dot-dashed lines*, spectra from 2006 are shown with *dashed lines*, and spectra from 2007 are shown with *solid lines*.

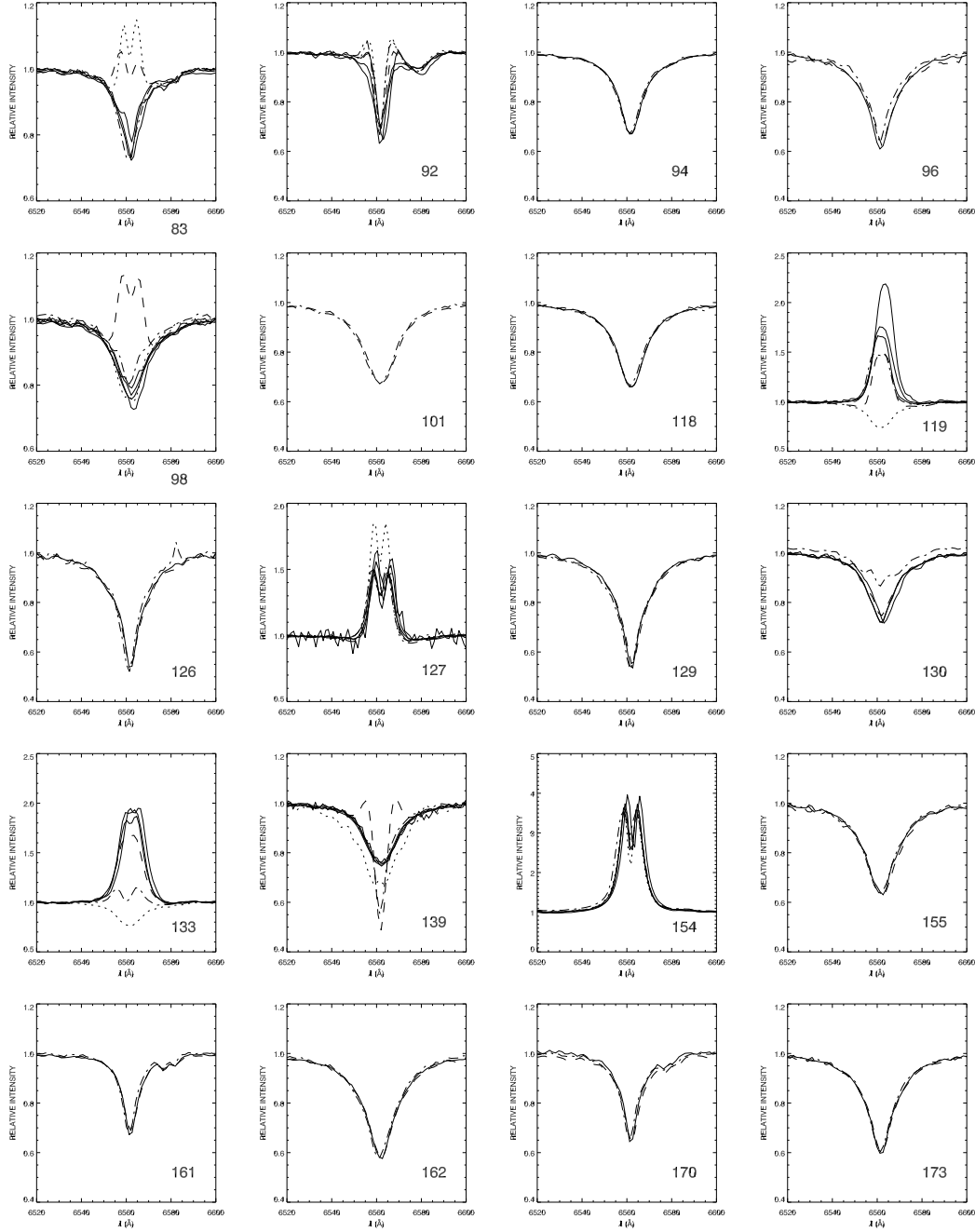


Fig. 2.— $H\alpha$ profiles in the same format as Fig. 1.

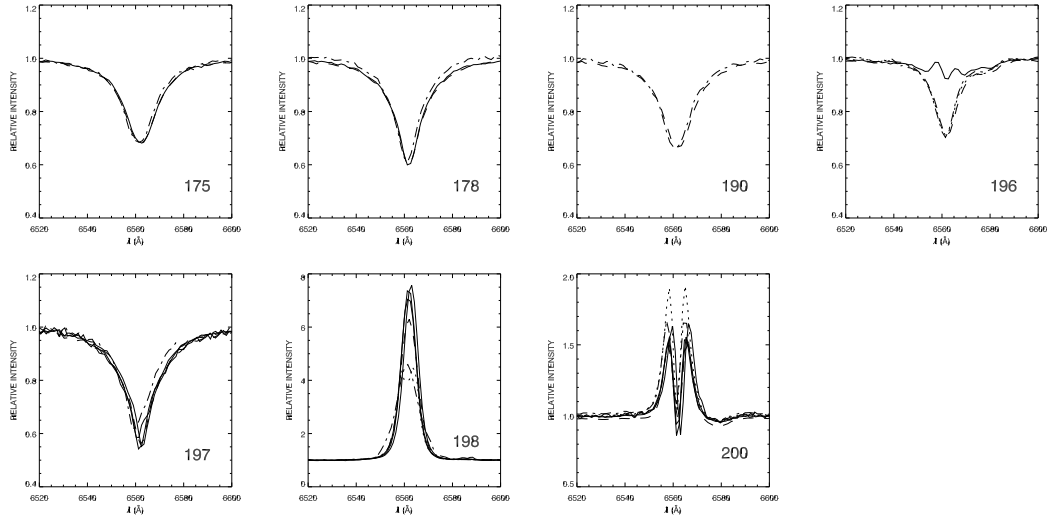


Fig. 3.— $H\alpha$ profiles in the same format as Fig. 1.

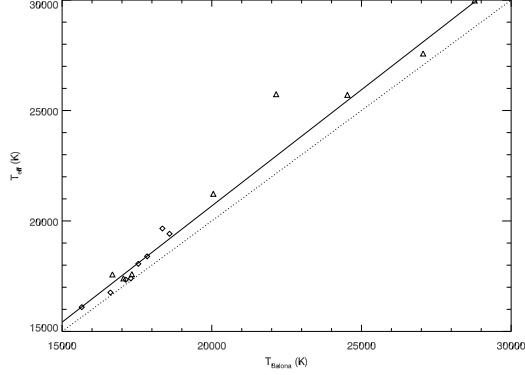


Fig. 4.— T_{eff} measured for the B-type temperature calibration stars from this work (*diamonds*) and from Napiwotzki (1993; *triangles*) compared to their calculated T_{Balona} (Balona 1984). A linear fit to the two temperature scales (*solid line*) and the 1:1 agreement (*dotted line*) are also shown.

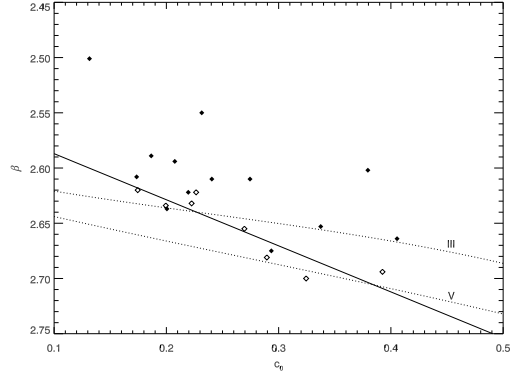


Fig. 5.— Strömberg c_0 index plotted against the β magnitude for the B-type temperature calibration stars from this work (*diamonds*). Be stars are also plotted (*filled diamonds*) to illustrate the contamination in β due to their disk emission. We also show the (c_0, β) relations for luminosity class V and III stars (Balona & Shobbrook 1984; *dotted lines*) and our linear fit to this evolving population (*solid line*).

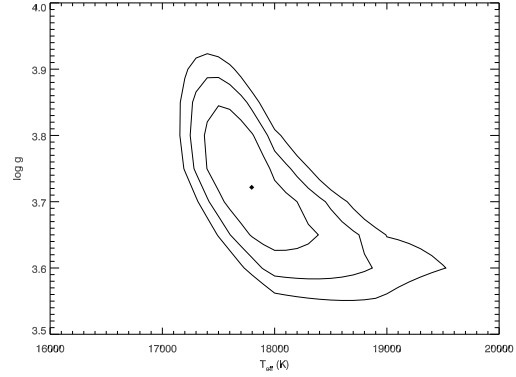


Fig. 6.— A contour plot of the 1σ , 2σ , and 3σ errors in the He I $\lambda 4388$ line fit for No. 31. We adopted the center of the 1σ error region as the best fit value, and the extent of this region indicates the sizes of the error bars for T_{eff} and $\log g$.

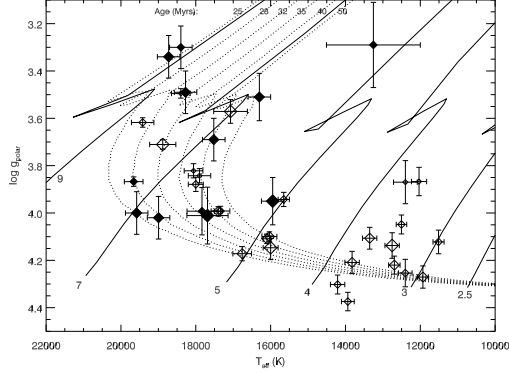


Fig. 7.— T_{eff} and $\log g_{\text{polar}}$ are plotted with the evolutionary tracks of Schaller et al. (1992) (*solid lines*) and isochrones of Lejeune & Schaerer (2001) (*dotted lines*). The zero-age MS mass of each evolutionary track is labeled along the bottom, and the age of each isochrone is labeled along the top. Normal B-type stars are shown as open diamonds while Be stars are filled diamonds, and each symbol size is proportional to the star's $V \sin i$.

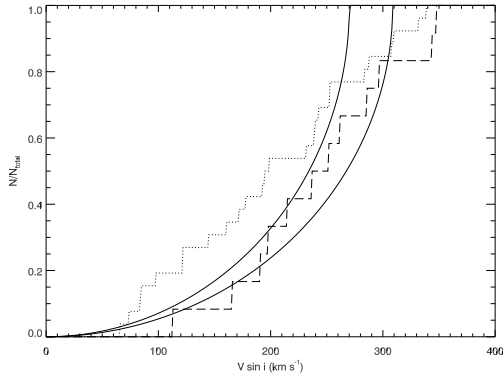


Fig. 8.— Cumulative distribution function of $V \sin i$ for the Be stars (*dashed line*) and the normal B-type stars (*dotted line*). Theoretical distributions of rapidly rotating stars with random orientation and $V = 0.7 V_{\text{crit}}$ and $0.8 V_{\text{crit}}$ are also shown (*solid lines*; assumes the mean value for the Be stars, $V_{\text{crit}} = 386 \text{ km s}^{-1}$).

TABLE 1
JOURNAL OF SPECTROSCOPY

UT Dates	Range (Å)	Resolving Power ($\lambda/\Delta\lambda$)	Number of Spectra	Telescope + Spectrograph	Slit Plate (μm)	Grating	Filter	Detector
2003 Mar 21 – 22	5490 – 6790	1800	20	CTIO 1.5m + Cassegrain	...	47/1	GG495	Loral 1K \times 1K
2005 Feb 2	4100 – 6900	1900	47	CTIO Blanco 4m + Hydra	200	KPGL3/1	...	SiTe 4K \times 2K
2006 May 13	3790 – 4708	3170	38	CTIO Blanco 4m + Hydra	...	KPGLD/2	BG39	SiTe 4K \times 2K
2006 May 14 – 15	5125 – 8000	1560	47	CTIO Blanco 4m + Hydra	...	KPGL3/1	...	SiTe 4K \times 2K
2007 May 4 – 5	5125 – 8000	2000	45	CTIO Blanco 4m + Hydra	200	KPGL3/1	...	SiTe 4K \times 2K
2007 Jan 20	5650 – 6790	1700	10	CTIO 1.5m + Cassegrain	...	47/1	GG495	Loral 1K \times 1K
2007 Jan 29	5650 – 6790	1700	2	CTIO 1.5m + Cassegrain	...	47/1	GG495	Loral 1K \times 1K
2007 Feb 2	5650 – 6790	1700	8	CTIO 1.5m + Cassegrain	...	47/1	GG495	Loral 1K \times 1K
2007 Apr 26	5650 – 6790	1700	5	CTIO 1.5m + Cassegrain	...	47/1	GG495	Loral 1K \times 1K
2007 Jun 9	5650 – 6790	1700	1	CTIO 1.5m + Cassegrain	...	47/1	GG495	Loral 1K \times 1K
2007 Jun 30	5650 – 6790	1700	9	CTIO 1.5m + Cassegrain	...	47/1	GG495	Loral 1K \times 1K
2007 Jul 3	5650 – 6790	1700	2	CTIO 1.5m + Cassegrain	...	47/1	GG495	Loral 1K \times 1K
2007 Jul 27 – 28	5650 – 6790	1700	7	CTIO 1.5m + Cassegrain	...	47/1	GG495	Loral 1K \times 1K

TABLE 2
H α EQUIVALENT WIDTHS

MG ID	WEBDA ID	W_λ (Å) (2003 Mar)	W_λ (Å) (2005 Feb)	W_λ (Å) (2006 May)	W_λ (Å) (2007 Jan/Feb)	W_λ (Å) (2007 Apr)	W_λ (Å) (2007 May)	W_λ (Å) (2007 June)	W_λ (Å) (2007 July)
2	3.24	4.07	3.93
16	169	...	4.28	4.26	3.84
23	9.22	9.37	7.59
25	291	3.62	3.18	5.30	-1.63, -1.06	0.42	1.04	1.42	...
27	146	5.14	5.38	5.69	4.74
31	151	2.91	3.99	0.57	-3.34, -5.94	-6.64	-6.80
36	13	...	8.46	8.56	6.93
41	130	...	4.88	5.28	4.41
42	178	...	6.07	6.02	5.22
45	8	4.69	4.98	5.10	4.35
47	15	-14.99	-11.33	-11.29	-8.11	...	-6.81	-5.61	-4.68
49	137	4.87	4.37	4.89	4.25
54	125	...	5.18	5.61	4.84
55	5.03	5.12	4.59
57	24	...	5.67	5.86	4.72
61	20	...	4.09	3.54	3.66	...	3.56	4.41	1.20
69	2.89	3.19	2.81
72	4	7.19	8.27	8.65	7.14	...	7.08	...	7.25
73	26	3.65	0.42	3.28	1.27	...	-0.35	...	-0.92
77	195	4.85	4.61	5.72	4.73
83	27	0.53	4.07	0.84	2.92	3.72	2.93
92	1	2.06	2.31	2.73	3.32	...	3.41	2.66	...
94	194	...	5.94	5.91	4.94
96	45	...	6.39	6.87	6.26
98	36	4.99	3.10	0.21	4.43	4.36	4.14	...	5.05
101	34	...	7.40	7.44
118	7.40	7.03	5.73
119	81	4.76	-5.48	-3.19	-6.53	...	-8.67	...	-12.83
126	7.46	8.49	6.86
127	53	-7.21	-4.95	-4.00	-4.19	...	-5.47	-5.60	-12.81
129	8.66	7.94	6.84
130	67	...	2.00	5.04	4.23	...	4.44	4.38	...
133	63	4.40	-1.15	-9.14	-11.62	...	-12.72	-12.40	...
139	204	8.48	5.46	4.24	4.51	4.50	4.42	5.54	...
154	88	-33.46	-40.07	-33.56	-34.37	...	-33.95	...	-36.16
155	7.92	7.90	6.38
161	70	...	3.92	4.19	3.61
162	9.15	9.23	7.45
170	94	...	4.81	5.26	4.17
173	233	...	7.79	7.92	6.62
175	218	...	6.67	6.74	6.01
178	213	...	6.32	7.71	6.35
190	260	...	6.81	6.86
196	239	4.52	4.32	4.39	1.46
197	253	...	7.65	8.85	7.04	...	7.09	...	7.66
198	264	-39.49	-43.40	-53.71	-52.77	...	-53.44	-54.69	...
200	240	-8.84	-6.66	-4.62	-4.88	...	-5.19	-5.76	...

TABLE 3
PHYSICAL PARAMETERS OF CLUSTER MEMBERS

	MG ID	$V \sin i$ (km s ⁻¹)	$\Delta V \sin i$ (km s ⁻¹)	T_{eff} (K)	ΔT_{eff} (K)	$\log g$	$\Delta \log g$	$\log g_{\text{polar}}$	M_{\star} (M_{\odot})	ΔM_{\star} (M_{\odot})	R_{\star} (R_{\odot})	ΔR_{\star} (R_{\odot})	V_{crit} (km s ⁻¹)
B stars:	2 ^a	307	5	17071	450	3.10	0.05	3.57	7.0	0.3	7.2	0.6	352
	16 ^a	144	7	19420	300	3.48	0.02	3.62	8.6	0.2	7.5	0.5	380
	27 ^a	287	6	16033	200	3.83	0.02	4.10	4.9	0.1	3.3	0.8	436
	36 ^a	283	22	11931	145	4.02	0.05	4.27	3.0	0.0	2.1	0.1	424
	41 ^a	84	7	17900	300	3.78	0.03	3.84	6.6	0.1	5.1	0.8	406
	42 ^a	239	5	16100	100	3.90	0.02	4.11	4.9	0.0	3.2	0.8	438
	49 ^a	252	9	17400	100	3.75	0.02	3.99	6.0	0.1	4.1	0.9	431
	54 ^a	192	9	17340	250	3.82	0.02	3.99	5.9	0.1	4.1	0.9	430
	55 ^a	121	6	18000	200	3.78	0.03	3.88	6.6	0.1	4.9	0.8	413
	57 ^a	238	8	16760	250	3.98	0.03	4.17	5.1	0.2	3.1	1.0	459
	61 ^{a,b}	331	8	18883	350	3.23	0.02	3.71	7.7	0.3	6.4	0.6	390
	77 ^a	338	10	16000	200	3.80	0.05	4.15	4.8	0.1	3.1	0.9	445
	94 ^a	177	5	15650	150	3.78	0.03	3.94	5.0	0.1	4.0	0.5	401
	96 ^a	121	5	13937	171	4.31	0.04	4.37	3.6	0.1	2.0	0.3	472
	101 ^a	309	14	12753	192	3.84	0.05	4.14	3.5	0.1	2.6	0.4	409
	118 ^a	242	9	13353	191	3.89	0.05	4.11	3.7	0.1	2.8	0.5	409
	126 ^a	83	9	12399	318	3.79	0.09	3.87	3.8	0.1	3.7	0.4	358
	129 ^a	97	27	12034	203	3.77	0.06	3.87	3.7	0.1	3.7	0.3	355
	155 ^a	231	11	12694	153	4.05	0.04	4.22	3.3	0.1	2.3	0.5	425
	161 ^a	73	7	18400	250	3.43	0.02	3.49	8.3	0.2	8.5	0.4	351
	162 ^a	194	11	11513	148	3.99	0.05	4.12	3.0	0.1	2.5	0.2	390
	170 ^a	65	6	18060	250	3.78	0.03	3.82	6.8	0.1	5.3	0.7	403
	173 ^a	171	7	14210	192	4.21	0.04	4.30	3.8	0.1	2.3	0.1	459
	175 ^a	252	13	13823	193	4.01	0.05	4.21	3.8	0.1	2.5	0.6	435
	178 ^a	160	12	12504	141	3.92	0.04	4.05	3.5	0.1	2.9	0.3	390
	197 ^{a,b}	198	15	12402	182	4.15	0.06	4.25	3.2	0.1	2.2	0.5	427
Be stars:	25 ^c	261	6	18995	301	4.02	0.09	4.02	6.6	0.1	4.1	0.9	450
	31 ^d	197	5	17834	400	3.82	0.10	3.99	6.2	0.2	4.2	1.0	435
	47 ^c	190	5	18399	301	3.30	0.09	3.30	9.3	0.1	11.3	2.3	323
	73 ^c	296	5	18274	301	3.49	0.09	3.49	8.2	0.1	8.5	1.8	349
	83 ^c	18817	301	3.31	0.09	3.31	9.9	0.1	11.5	2.4	329
	92 ^c	214	17	18725	301	3.34	0.09	3.34	9.5	0.1	10.8	2.3	332
	98 ^c	16890	301	3.84	0.10	3.84	6.2	0.1	4.9	1.0	398
	119 ^c	17792	301	3.75	0.09	3.75	6.8	0.1	5.8	1.2	387
	127 ^d	347	5	17687	550	3.61	0.12	4.01	6.1	0.3	4.0	1.0	437
	130 ^c	285	7	17519	301	3.69	0.09	3.69	6.9	0.1	6.2	1.3	375
	133 ^c	18564	301	3.53	0.09	3.53	8.3	0.1	8.1	1.7	358
	139 ^c	343	12	15945	301	3.95	0.10	3.95	5.2	0.1	4.0	0.8	406
	154 ^c	112	29	13254	1254	3.29	0.18	3.29	5.6	0.3	8.8	1.8	282
	196 ^a	165	5	19660	250	3.73	0.02	3.87	7.6	0.2	5.3	1.1	426
	198 ^c	251	6	19580	301	4.00	0.09	4.00	7.0	0.1	4.4	0.9	449
	200 ^c	236	12	16301	301	3.51	0.10	3.51	6.8	0.1	7.5	1.6	337

^a T_{eff} and $\log g$ measured from H γ line fit.

^bParameters are unreliable since the star is a suspected SB2.

^c T_{eff} and $\log g$ measured from Strömgren photometry.

^d T_{eff} and $\log g$ measured from He I line fits.

TABLE 4
ESTIMATED SIZES OF BE STAR DISKS

MG ID	HJD– 2,450,000	Assumed V/V_{crit}	i (deg)	$\log \rho_0$ (g cm ^{−3})	R_{disk}/R_*	M_{disk} ($10^{-11} M_{\odot}$)	$\Delta M_{\text{disk}}/\Delta t$ ($10^{-11} M_{\odot} \text{ yr}^{-1}$)
25	2720.825	0.7	64.9	−12.2	2.3	41.9	...
	3403.79	−12.1	2.5	44.3	1.3
	3870	−12.3	1.6	30.6	−10.7
	4120.664	−12.0	3.8	66.1	51.7
	4129.743	−12.0	3.7	63.7	−92.7
	4216.493	−12.0	3.3	57.5	−26.3
	4225.66	−12.1	3.1	54.7	−110.0
	4260.635	−12.1	3.0	53.0	−17.8
31	2720.744	0.7	40.5	−12.1	2.5	19.8	...
	3403.79	−12.2	2.1	17.2	−1.4
	3870	−12.0	3.0	24.6	5.8
	4120.677	−11.9	3.7	31.4	9.9
	4129.771	−11.9	4.1	35.0	142.4
	4216.512	−11.9	4.1	35.7	3.3
	4225.66	−11.9	4.2	35.9	6.7
47	2719.557	0.7	40.8	−11.8	4.5	72.3	...
	3403.79	−11.8	4.4	70.3	−1.1
	3870	−11.8	4.4	70.2	0.0
	4133.656	−11.9	4.2	66.3	−5.4
	4225.66	−11.9	4.1	64.1	−8.8
	4281.495	−11.9	4.0	61.7	−15.7
	4309.466	−11.9	3.9	59.5	−28.5
73	2719.567	0.7	73.1	−12.2	2.5	16.7	...
	3403.79	−12.0	3.5	23.0	3.4
	3870	−12.1	2.6	17.5	−4.3
	4120.711	−12.1	3.3	21.5	5.8
	4225.66	−12.0	3.7	24.3	9.9
	4308.554	−12.0	3.9	25.3	4.1
92	2719.629	0.7	48.9	−12.1	2.7	50.4	...
	3403.79	−12.1	2.6	49.1	−0.7
	3870	−12.1	2.5	47.0	−1.7
	4133.668	−12.1	2.3	43.9	−4.3
	4225.66	−12.2	2.3	43.4	−1.9
	4281.510	−12.1	2.5	47.3	25.9
127	2719.759	0.8	80.1	−11.9	5.6	30.7	...
	3403.79	−11.9	5.2	28.5	−1.2
	3870	−11.9	5.0	27.4	−0.9
	4133.680	−11.9	5.0	27.6	0.3
	4225.66	−11.9	5.3	29.1	5.8
	4281.524	−11.9	5.3	29.2	0.9
	4309.495	−11.8	6.1	33.8	59.9
130	3403.79	0.7	63.5	−12.1	3.0	11.9	...
	3870	−12.3	1.8	7.7	−3.3
	4120.750	−12.2	2.2	9.0	1.9
	4225.66	−12.2	2.1	8.7	−1.1
	4281.540	−12.2	2.1	8.8	0.6
139	2720.796	0.9	50.6	...	0.0	0.0	...
	3403.79	−12.3	1.8	1.7	0.9
	3870	−12.2	2.3	2.2	0.4
	4120.770	−12.2	2.2	2.1	−0.1

TABLE 4—*Continued*

MG ID	HJD— 2,450,000	Assumed V/V_{crit}	i (deg)	$\log \rho_0$ (g cm $^{-3}$)	$R_{\text{disk}}/R_{\star}$	M_{disk} ($10^{-11}M_{\odot}$)	$\Delta M_{\text{disk}}/\Delta t$ ($10^{-11}M_{\odot}$ yr $^{-1}$)
	4216.632	−12.2	2.2	2.2	0.0
	4225.66	−12.2	2.3	2.2	0.0
	4281.572	−12.3	1.8	1.7	−3.2
196	3870	0.7	33.5	...	0.0	0.0	...
	4225.66	−12.1	2.6	15.0	15.4
198	2720.658	0.7	69.9	−11.9	5.0	253.4	...
	3403.79	−11.9	4.9	248.9	−2.4
	3870	−11.9	4.7	238.7	−8.0
	4133.732	−11.9	4.7	239.5	1.1
	4225.66	−11.9	4.7	238.9	−2.4
	4281.589	−11.9	4.7	237.8	−7.1
200	2720.637	0.7	46.2	−11.8	4.8	9.9	...
	3403.79	−11.9	4.6	9.4	−0.3
	3870	−11.9	4.3	8.7	−0.5
	4133.741	−11.9	4.3	8.8	0.1
	4225.66	−11.9	4.4	8.9	0.4
	4281.599	−11.9	4.5	9.1	1.2